

Optimized Si_3N_4 grating couplers for relaxed alignment requirements under flood illumination

DAAN MARTENS,^{1,2,*} GENGHUA DONG,^{1,2} AND PETER BIENSTMAN^{1,2}

¹Photonics Research Group, INTEC, Ghent University—IMEC, Technologiepark-Zwijnaarde 15, 9000 Ghent, Belgium

²Center for Nano- and Biophotonics (NB-Photonics), Ghent University, Technologiepark-Zwijnaarde 15, 9000 Ghent, Belgium

*Corresponding author: daand.martens@ugent.be

Received 25 October 2016; revised 19 December 2016; accepted 10 January 2017; posted 12 January 2017 (Doc. ID 279164); published 2 February 2017

Grating couplers are essential building blocks to integrated photonic circuits, as they allow surface access to the photonic chip. They are most commonly used in combination with an optical fiber, requiring precise alignment, resulting in a high instrumentation cost. In this paper, an alternate use is proposed: by flood illuminating part of the chip surface, the alignment conditions can be relaxed. The grating coupler parameters were optimized for this coupling method. The novel grating couplers were fabricated in Si_3N_4 and characterized through flood illumination measurements. At peak wavelength as well as within a 20 nm interval, the coupled power was increased considerably over a smaller coupler, by a factor of 6 and 4.5, respectively. The influence on bandwidth and the required precision of coupling angle were also investigated. These optimized designs for flood illumination can provide a cost-efficient coupling mechanism for numerous applications. © 2017 Optical Society of America

OCIS codes: (060.3735) Fiber Bragg gratings; (050.6624) Subwavelength structures; (130.1750) Components.

<https://doi.org/10.1364/AO.56.001286>

1. INTRODUCTION

Grating couplers are one of the essential building blocks of numerous integrated photonic systems. In contrast to edge coupling, they do not require cleaving and polishing of the chip facets and allow access from anywhere on the surface rather than only at the edge. The most common application is coupling from optical fibers, and such devices have been well established in silicon-on-insulator technology in the telecommunications range [1,2], and are finding a breakthrough in other waveguide ranges and material platforms as well [3–6].

One advantage of these grating couplers is their relatively high alignment tolerance compared to edge coupling mechanisms [7,8]. Nevertheless, a micrometer offset of the fiber relative to the grating coupler still causes several decibels of additional loss [9], requiring expensive stages to ensure adequate alignment. Certain applications, in particular point-of-care diagnostics and environmental monitoring [10], require a more low-cost approach for the chip interface. Such a cost-effective system can be achieved with grating couplers by making the input light spot on the chip surface much larger than the input grating couplers, a system called flood illumination, resulting in strongly relaxed alignment conditions. While most research on grating couplers focuses heavily on fiber-to-chip coupling, grating couplers have been successfully used in such a flood illumination scheme for relaxed alignment conditions as part of a sensing circuit in [11], but the grating design was not

specifically adapted to this readout scheme. In this work we present the optimization of a grating coupler, specifically for flood illumination. As a material platform, Si_3N_4 is selected, as it allows operation in the very near-infrared (VNIR) wavelength region (700–1000 nm). This region is of particular interest for sensing and monitoring applications, due to both the availability of high-quality, low-cost sources as well as the presence of the therapeutic window due to the low absorption of both blood and water.

In this emerging material platform, low-loss waveguides have been developed [12]. Fiber-to-chip grating couplers exist in both the telecommunications range [13–15] as well as in the visible [4] and VNIR wavelength ranges [3]. The latter, which were developed in our group, serve as a starting point for this optimization. The goal of such an optimization depends on the specific application, and here the authors intend to use this coupling scheme with on-chip spectral filters with a bandwidth of 20 nm. Therefore, while most conclusions will be generally valid, our main target is optimizing the power within a 20 nm window.

2. SIMULATION RESULTS

The main goal of the finite-difference time-domain method simulations presented in this section is to assess the effect of increasing the number of periods, as this influences both power and bandwidth, while the width theoretically only influences

the power. We therefore limit the simulation to two dimensions, assuming an infinitely wide grating coupler. Similar to our fabricated grating couplers, discussed in the next section, the waveguide consisted of an airclad 220 nm Si₃N₄ layer, with a buried oxide layer of 2.3 μm on top of a Si substrate. *A priori*, both etch depth and fill factor were kept at 50%, the latter to facilitate the first diffraction order, the former again to match the fabrication parameters. As a source, a plane wave was chosen, as under flood illumination operation occurs in the far-field regime, which for most source types can be locally approximated by a plane wave. The source angle used in this simulation was 15°. Of course, the general conclusions are valid for other parameters and material platforms as well.

Figures 1 and 2 show the transmission power and the bandwidth of the grating coupler, as a function of its length, expressed in number of periods. The former shows both the full width at half-maximum (FWHM) and the peak transmission power, normalized to the grating coupler optimized for fiber coupling, which has 20 periods. The figure indicates that for increasing length, the power coupled to the waveguide increases. This is intuitively clear, as comparatively more power hits the surface of the grating coupler. Simultaneously, the

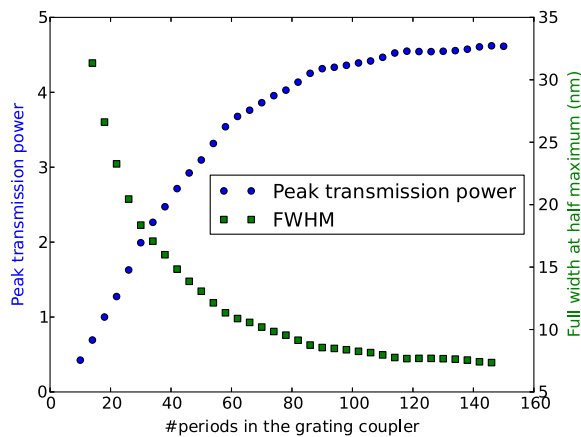


Fig. 1. Peak power and bandwidth under flood illumination as a function of grating coupler length.

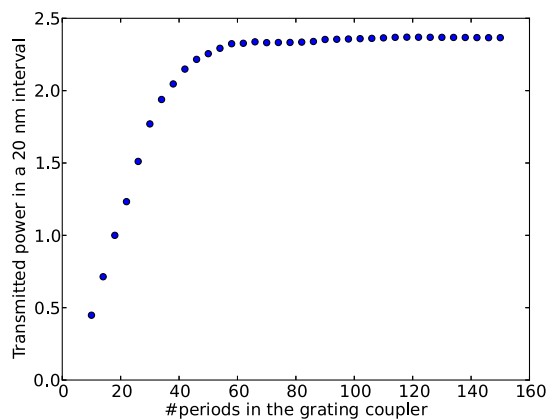


Fig. 2. Total coupled power in a 20 nm interval as a function of grating coupler length.

FWHM decreases as a longer grating coupler better approaches a perfect, infinitely long grating coupler, which has an infinitely narrow spectrum.

In combination, these phenomena result in the data shown in Fig. 2, which displays the target of the optimization, the total coupled power in a 20 nm interval. It also saturates, sooner even than the peak transmission power as the decreasing FWHM counteracts the former. This indicates that for an optimization of the power within a 20 nm interval, the optimum length lies around 3 times the length of the original coupler, as further periods do not improve the total power, and reduce the FWHM and hence the power at the edge of the wavelength range. For optimizing transmission at peak wavelength, such a compromise is not necessary, and only footprint considerations need to be made.

To quantify the results of these simulations, their peak transmission values were normalized with respect to the power directly incident onto the grating coupler. The results are shown in Fig. 3 and indicate an initial increase of up to 22% for a grating measuring 40 periods, after which the efficiency gradually decreases, as the additional periods contribute little while the incident power still increases linearly with grating length. Because of the flood illumination regime, the efficiency with respect to the total source power will be considerably lower, depending on the ratio of the spot size to the size of the grating coupler. Similarly, it is not straightforward to generally simulate (or measure) the position dependence, as this depends only on the characteristics of the spot caused by the flood illumination. For these simulations, where a perfect plane wave was assumed, the result is, of course, independent of the source position.

As a second step, we verify the effect of the etch depth, as the contributions of the added length can improve for a weaker grating. The integrated power in a 20 nm interval is given for different etch depths in Fig. 4. As expected, the saturation occurs later for weaker grating couplers. The saturation value is highest for an etch of 64 nm, but the difference with other etch depths remains below 20%, except for extremely shallow or deep etches. Considering that shallower etched gratings might

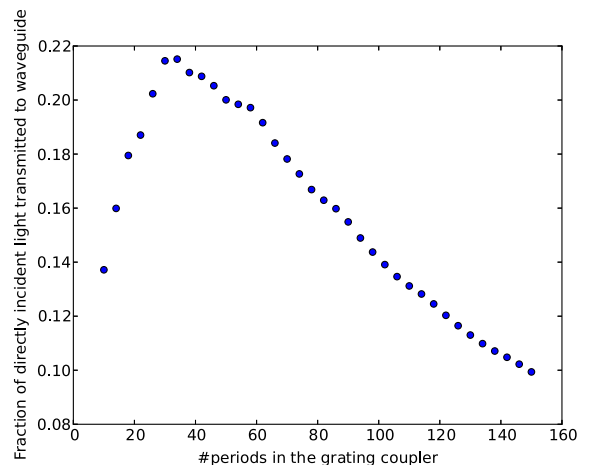


Fig. 3. Transmitted power normalized with respect to power directly incident on grating coupler.

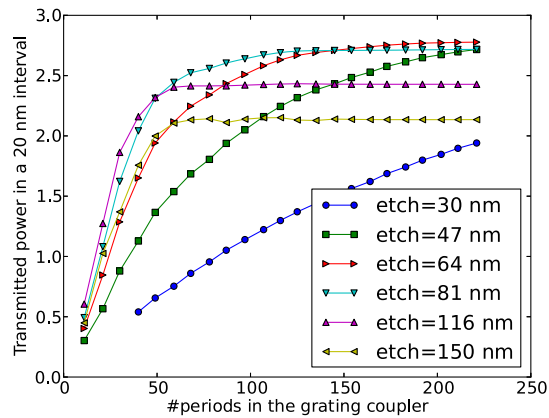


Fig. 4. Transmitted power in a 20 nm interval as a function of grating length for different etch depths.

suffer comparatively more from the nonuniformity generated by fabrication imperfection, the practical improvement is expected to be even lower.

3. EXPERIMENTAL RESULTS

The devices were fabricated in a 220 nm Si_3N_4 platform [12]. The etch depth in this fabrication scheme was fixed to 110 nm, 50%. Similar to the simulations, the fill factor was kept at 50% as well to focus on the first diffraction and limit the footprint of the parameter sweep. Grating coupler length and width were both swept. All grating couplers had linear tapers. The grating couplers were designed for coupling light around 850 nm at 15° , due to an external requirement of the system in which the couplers are to be integrated. The grating couplers were measured under 15° ; on the input side they were flood illuminated through a free-space broadband source, and on the output side a regular grating coupler was implemented, measured through a fiber. A short waveguide with negligible loss connected both grating couplers [12]. After dividing by the source spectrum as well as the small grating coupler spectrum, a Savitzky–Golay filter [16] was applied to eliminate the unwanted resonances caused by cavities within the source. To further reduce their effect as well as the effect of noise, a Gaussian fit was applied to the obtained spectrum of the large grating coupler, and the presented results are extracted from those Gaussians. An example of such a Gaussian fit is shown in Fig. 5.

The results for transmitted intensity at peak wavelength are shown in Fig. 6, where similar to the simulations, the values are normalized with respect to the grating coupler optimized for fiber coupling, which has 20 periods and a width of 10 μm . The displayed results were obtained by averaging over measurement data from six chips. By purely increasing the length, the peak transmission can be increased by about a factor of 1.8; this is similar for all grating widths, indicating the expected independence of length and width. The improvement is considerably lower compared to the simulation where a factor of close to 5 was achieved, probably due to the fabrication imperfections, which become increasingly significant for larger devices. Similar to the simulation, for a 50% etch depth saturation begins to show for 80 periods. Increasing the width results in a linear

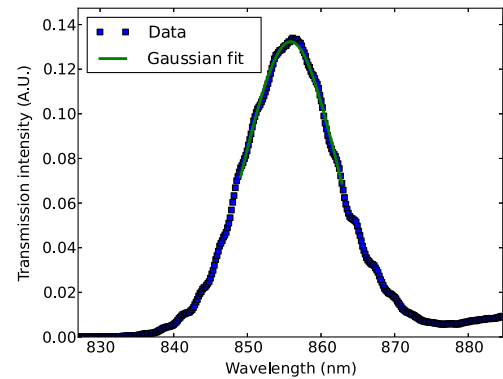


Fig. 5. Data after application of Savitzky–Golay filter and Gaussian fit.

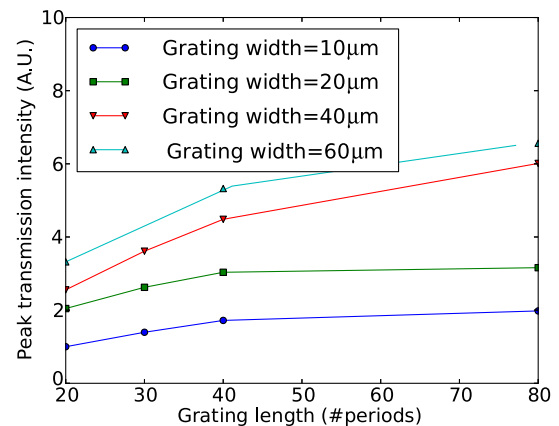


Fig. 6. Measured peak intensity as a function of grating length.

increase in transmitted power, with slight saturation for wider devices, possibly due to higher taper losses and stronger influence of fabrication imperfections. By increasing the width by a factor of 6, the peak transmitted power increases by over a factor of 3. Hence, by combining lengthening and widening, the power at peak wavelength is increased by a factor of 6.

The influence on the broadband behavior was also investigated. As expected, the width did not influence the FWHM at all, while a longer waveguide causes a more narrow transmission spectrum. This is illustrated in Fig. 7 where boxplots are given of the FWHM as a function of length, including data from all the measured widths, ranging from 10 to 60 μm . Because fabrication affected the FWHM differently for different wafer locations, the values were normalized with respect to the smallest grating coupler, similar to previous sections. The average absolute FWHMs were 20.0, 15.7, and 12.4 nm, respectively. The first value, for short grating couplers, matches that of the simulation in Fig. 1, but the decrease in bandwidth for longer grating couplers is less severe, probably again due to fabrication imperfections. Figure 8 shows the integrated power over a 20 nm interval, illustrating the same behavior as Fig. 6, but with a stronger saturation in length, resulting in a total improvement of over a factor of 4.

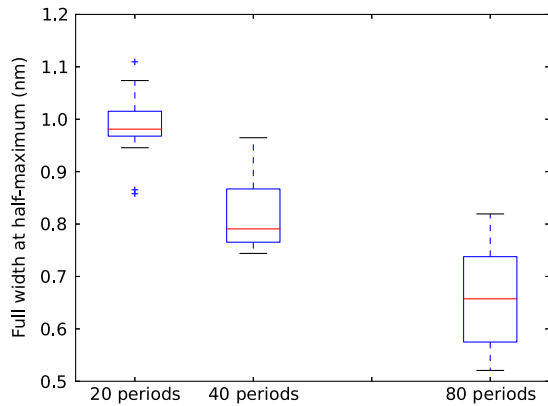


Fig. 7. Boxplot of full width at half-maximum of experimental spectra.

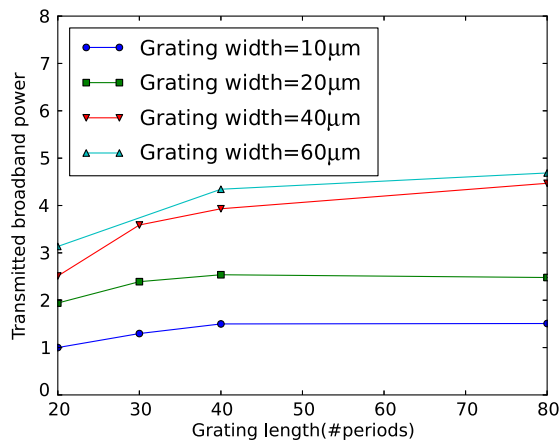


Fig. 8. Total coupled power in a 20 nm interval as a function of grating coupler length.

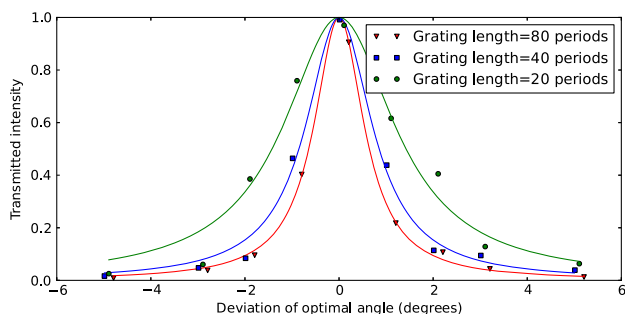


Fig. 9. Experimental transmitted intensity at a fixed wavelength as a function of coupling angle.

The angle dependence was also investigated, and the peak wavelength shifts about 4.5 nm per degree, for all grating dimensions. Therefore, the intensity loss for any given wavelength scales solely with the FWHM, indicating that for applications where high power at a specific wavelength is required, the angle accuracy requirements become more stringent for longer grating couplers. This is illustrated in Fig. 9, where

experimental results are shown. The transmitted intensity is plotted, for a fixed wavelength and varying angle. A Lorentzian fit is added to emphasize the trend. For a misalignment of 1°, the power drops to 30% for the longest grating, while remaining at 67% for the shorter grating coupling. This stronger angle dependence is an important consideration for usage in a low-cost readout, where angle deviations from the optimum may be prevalent. Similar to this, in a practical device a compromise has to be made for the flood illumination between a large spot to obtain the desired tolerance of alignment on one hand, and a small spot to limit the power loss through the inherently power-inefficient flood illumination coupling mechanism on the other hand. As an example of such a successful compromise, these grating couplers were used in the photonic integrated sensing circuit described in [17], where bulk characterization was performed through flood illumination by a 12 mW superluminescent diode (SLD).

4. CONCLUSION

We have designed and measured an optimized grating coupler, for flood illumination instead of coupling to and from optical fibers. These gratings were fabricated in the Si_3N_4 material platform, where the improvement in coupled power over a regular grating coupler was a factor of 6 at peak wavelength and a factor of 4 over a 20 nm interval, due to the effect of the decreasing FWHM with increasing length. Based on the simulations, further improvement is possible without complicating the fabrication procedure by using a weaker grating than the 50% that was used here. In general, depending on the application, compromises are needed between both the width and the peak power of the transmission of the grating coupler, as well as between the alignment tolerances and the power efficiency of the flood illumination scheme. This compromise is facilitated by adapting the grating couplers, as they can limit the power losses for flood illumination, and hence relax requirements for both alignment and optical source, while maintaining surface access to the chip. This low-cost coupling with minimized losses is a vital feature for applications where the success largely depends on cost-efficiency, such as point-of-care sensors.

Funding. Seventh Framework Programme (FP7) (Pocket 610389).

REFERENCES

1. G. Roelkens, D. Vermeulen, F. Van Laere, S. Selvaraja, S. Scheerlinck, D. Taillaert, W. Bogaerts, P. Dumon, D. Van Thourhout, and R. Baets, "Bridging the gap between nanophotonic waveguide circuits and single mode optical fibers using diffractive grating structures," *J. Nanosci. Nanotechnol.* **10**, 1551–1562 (2010).
2. A. Mekis, S. Gloeckner, G. Masini, A. Narasimha, T. Pinguet, S. Sahni, and P. De Dobbelaere, "A grating-coupler-enabled CMOS photonics platform," *IEEE J. Sel. Top. Quantum Electron.* **17**, 597–608 (2011).
3. A. Subramanian, S. Selvaraja, P. Verheyen, A. Dhakal, K. Komorowska, and R. Baets, "Near-infrared grating couplers for silicon nitride photonic wires," *IEEE Photon. Technol. Lett.* **24**, 1700–1703 (2012).
4. S. Romero-García, F. Merget, F. Zhong, H. Finkelstein, and J. Witzens, "Visible wavelength silicon nitride focusing grating coupler with AlCu/TiN reflector," *Opt. Lett.* **38**, 2521–2523 (2013).

5. N. Hattasan, B. Kuyken, F. Leo, E. M. P. Ryckeboer, D. Vermeulen, and G. Roelkens, "High-efficiency SOI fiber-to-chip grating couplers and low-loss waveguides for the short-wave infrared," *IEEE Photon. Technol. Lett.* **24**, 1536–1538 (2012).
6. D. Duval, J. Osmond, S. Dante, C. Domínguez, and L. M. Lechuga, "Grating couplers integrated on Mach-Zehnder interferometric biosensors operating in the visible range," *IEEE Photon. J.* **5**, 3700108 (2013).
7. L. Chen, C. R. Doerr, Y.-K. Chen, and T.-Y. Liow, "Low-loss and broadband cantilever couplers between standard cleaved fibers and high-index-contrast Si_3N_4 or Si waveguides," *IEEE Photon. Technol. Lett.* **22**, 1744–1746 (2010).
8. M. Pu, L. Liu, K. Yvind, and J. M. Hvam, "Ultra-low-loss inverted taper coupler for silicon-on-insulator ridge waveguide," *Opt. Commun.* **283**, 3678–3682 (2010).
9. D. Taillaert, F. Van Laere, M. Ayre, W. Bogaerts, D. Van Thourhout, P. Bienstman, and R. Baets, "Grating couplers for coupling between optical fibers and nanophotonic waveguides," *Jpn. J. Appl. Phys.* **45**, 6071–6077 (2006).
10. A. F. Gavela, D. G. García, J. C. Ramirez, and L. M. Lechuga, "Last advances in silicon-based optical biosensors," *Sensors* **16**, 285 (2016).
11. S. Janz, D.-X. Xu, M. Vachon, N. Sabourin, P. Cheben, H. McIntosh, H. Ding, S. Wang, J. H. Schmid, A. Delâge, J. Lapointe, A. Densmore, R. Ma, W. Sinclair, S. M. Logan, R. MacKenzie, Q. Y. Liu, D. Zhang, G. Lopinski, O. Mozenson, M. Gilmour, and H. Tabor, "Photonic wire biosensor microarray chip and instrumentation with application to serotyping of *Escherichia coli* isolates," *Opt. Express* **21**, 4623–4637 (2013).
12. A. Subramanian, P. Neutens, A. Dhakal, R. Jansen, T. Claes, X. Rottenberg, F. Peyskens, S. Selvaraja, P. Helin, B. Du Bois, K. Leyssens, S. Severi, P. Deshpande, R. Baets, and P. Van Dorpe, "Low-loss singlemode PECVD silicon nitride photonic wire waveguides for 532–900 nm wavelength window fabricated within a CMOS pilot line," *IEEE Photon. J.* **5**, 2202809 (2013).
13. C. R. Doerr, L. Chen, Y.-K. Chen, and L. L. Buhl, "Wide bandwidth silicon nitride grating coupler," *IEEE Photon. Technol. Lett.* **22**, 1461–1463 (2010).
14. H. Zhang, C. Li, X. Tu, X. Luo, M. Yu, and P. Guo-Qiang Lo, "High efficiency silicon nitride grating coupler," *Appl. Phys. A* **115**, 79–82 (2014).
15. G. Maire, L. Vivien, G. Sattler, A. Kaźmierczak, B. Sanchez, K. B. Gylfason, A. Griol, D. Marris-Morini, E. Cassan, D. Giannone, H. Sohlström, and D. Hill, "High efficiency silicon nitride surface grating couplers," *Opt. Express* **16**, 328–333 (2008).
16. A. Savitzky and M. J. E. Golay, "Smoothing and differentiation of data by simplified least squares procedures," *Anal. Chem.* **36**, 1627–1639 (1964).
17. D. Martens, A. Stassen, W. Van Roy, and P. Bienstman, "Novelty low-cost integrated photonic biosensor using broadband source and on-chip spectral filter," in *Proceedings of IEEE Photonics Society Benelux* (2015), pp. 173–176.